NAVAL POSTGRADUATE SCHOOL

MONTEREY, CALIFORNIA

THESIS

FINITE ELEMENT MODELING AND LONG-WAVE INFRARED IMAGING FOR DETECTION AND IDENTIFICATION OF BURIED OBJECTS

by

Heather P. Tilley

December 2017

Thesis Advisor: Fabio Alves
Co-Advisor: Gamani Karunasiri

THIS PAGE INTENTIONALLY LEFT BLANK

REPORT DOCUMENTATION PAGE			*Form Approved OMB No. 0704–0188*

1. AGENCY USE ONLY *(Leave blank)*	**2. REPORT DATE** December 2017	**3. REPORT TYPE AND DATES COVERED** Master's thesis

4. TITLE AND SUBTITLE FINITE ELEMENT MODELING AND LONG-WAVE INFRARED IMAGING FOR DETECTION AND IDENTIFICATION OF BURIED OBJECTS	**5. FUNDING NUMBERS**
6. AUTHOR(S) Heather P. Tilley	
7. PERFORMING ORGANIZATION NAME(S) AND ADDRESS(ES) Naval Postgraduate School Monterey, CA 93943-5000	**8. PERFORMING ORGANIZATION REPORT NUMBER**
9. SPONSORING /MONITORING AGENCY NAME(S) AND ADDRESS(ES) N/A	**10. SPONSORING / MONITORING AGENCY REPORT NUMBER**

11. SUPPLEMENTARY NOTES The views expressed in this thesis are those of the author and do not reflect the official policy or position of the Department of Defense or the U.S. Government. IRB number ____N/A____.

12a. DISTRIBUTION / AVAILABILITY STATEMENT Approved for public release. Distribution is unlimited.	**12b. DISTRIBUTION CODE**

13. ABSTRACT (maximum 200 words)

Detection of buried improvised explosive devices (IED) represents a complex threat to U.S. forces. This thesis explores the potential use of infrared images combined with finite element models to detect buried objects in soil. Initially, computer simulations using COMSOL Multiphysics software implemented a range of heat transfer dynamics to assess the feasibility of this approach. Then, an experimental setup was constructed to measure the surface temperature profile of a sandbox containing buried objects using a long-wave infrared camera. Images were recorded for several days under ambient conditions to determine detection capability for various attributes describing the buried object (shape, size, material and depth) and correlation to time of day. Best detection of buried objects corresponded to shallow depths for observed intervals where maxima/minima ambient temperatures coincided with expected diurnal cycling effects. Thermal contrast in the sand surrounding the buried object was not distinguishable at depths greater than eight cm. Utilizing a technique that extracted a surface intensity profile and fitted against simulated data for various soft metals (thermal conductivities and densities) indicated the potential ability to estimate a buried object's material composition. The preliminary results of the research indicate that infrared imaging could be used for passive detection of shallowly buried objects.

14. SUBJECT TERMS FEM simulations, passive detection, stand-off detection, image processing, counter-IED research, surface temperature maps	**15. NUMBER OF PAGES** 63
	16. PRICE CODE

17. SECURITY CLASSIFICATION OF REPORT	**18. SECURITY CLASSIFICATION OF THIS PAGE**	**19. SECURITY CLASSIFICATION OF ABSTRACT**	**20. LIMITATION OF ABSTRACT**
Unclassified	Unclassified	Unclassified	UU

NSN 7540–01-280-5500 Standard Form 298 (Rev. 2–89) Prescribed by ANSI Std. 239–18

THIS PAGE INTENTIONALLY LEFT BLANK

Approved for public release. Distribution is unlimited.

FINITE ELEMENT MODELING AND LONG-WAVE INFRARED IMAGING FOR DETECTION AND IDENTIFICATION OF BURIED OBJECTS

Heather P. Tilley
Lieutenant, United States Navy
B.S., University of Texas, Tyler, 2011

Submitted in partial fulfillment of the
requirements for the degree of

MASTER OF SCIENCE IN COMBAT SYSTEMS TECHNOLOGY

from the

NAVAL POSTGRADUATE SCHOOL
December 2017

Approved by: Fabio Alves
Thesis Advisor

Gamani Karunasiri
Co-Advisor

Kevin B. Smith
Chair, Department of Physics

THIS PAGE INTENTIONALLY LEFT BLANK

ABSTRACT

Detection of buried improvised explosive devices (IED) represents a complex threat to U.S. forces. This thesis explores the potential use of infrared images combined with finite element models to detect buried objects in soil. Initially, computer simulations using COMSOL Multiphysics software implemented a range of heat transfer dynamics to assess the feasibility of this approach. Then, an experimental setup was constructed to measure the surface temperature profile of a sandbox containing buried objects using a long-wave infrared camera. Images were recorded for several days under ambient conditions to determine detection capability for various attributes describing the buried object (shape, size, material and depth) and correlation to time of day. Best detection of buried objects corresponded to shallow depths for observed intervals where maxima/ minima ambient temperatures coincided with expected diurnal cycling effects. Thermal contrast in the sand surrounding the buried object was not distinguishable at depths greater than eight cm. Utilizing a technique that extracted a surface intensity profile and fitted against simulated data for various soft metals (thermal conductivities and densities) indicated the potential ability to estimate a buried object's material composition. The preliminary results of the research indicate that infrared imaging could be used for passive detection of shallowly buried objects.

THIS PAGE INTENTIONALLY LEFT BLANK

TABLE OF CONTENTS

THIS PAGE INTENTIONALLY LEFT BLANK

LIST OF FIGURES

LIST OF ACRONYMS AND ABBREVIATIONS

C-IED	counter improvised explosive device
COTS	commercial off the shelf
DOD	Department of Defense
FE	finite element
FEM	finite element model
IED	improvised explosive device
IR	infrared
LWIR	long-wave infrared
MWIR	mid-wave infrared
NIR	near infrared
NPS	Naval Postgraduate School
NQR	nuclear quadrupole resonance
RH	relative humidity
SRL	Sensor Research Laboratory at the Naval Postgraduate School
SWIR	short-wave infrared
TTPs	tactics, techniques, and procedures

THIS PAGE INTENTIONALLY LEFT BLANK

ACKNOWLEDGMENTS

I would like to take this space provided and express my sincerest gratitude to my thesis advisors, Dr. Karunasiri and Dr. Alves, who shared their experience and time, and continually guided me toward crossing the graduate school finish line. To my research team, I express my appreciation for your efforts in contributing to this research endeavor.

To my wife, April, your unwavering love and support served as my compass, compassionately directing me toward calmer waters. I am forever thankful for the winds of change that brought us together. I can scarcely imagine trying to navigate these waters without you by my side. My naval training would help some in this regard, but had it been land navigation, you know how I would fare.

THIS PAGE INTENTIONALLY LEFT BLANK

I. INTRODUCTION

Detection of buried energetics represents a complex, dynamic problem which threatens U.S. forces and grows in sophistication with the adversary's ingenuity. Simply speaking, detection and clearance techniques have not made consistent and significant advancements required to counter emerging improvised explosive device (IED) threats that pervade combat theaters abroad.

Presently, many commercial control measures are under development, but a comprehensive detection system capable of identifying and classifying an IED with high fidelity, and at an adequate standoff distance, is not yet in place. As an example, the Tactics, Techniques, and Procedures (TTPs) utilized in today's combat theater exhibit continued reliance on traditional detection technology -- metal detectors which can easily be deceived. An array of countermeasures, methodologies, and tactics developed within the past few decades have had some positive impact. However, mature technologies aided in conjunction with one or more traditional detection means, like the metal detector, have not propelled the end user much further beyond manually probing and prodding the suspect area, nor significantly improved standoff ranges.

How can the Department of Defense (DOD) ensure innovation, stay ahead of the threat, and develop timely and effective counter improvised explosive device (C-IED) solutions to better close the capabilities gap?

To date, a wide array of technologies and methodologies have been explored to perform this task. One unifying theme appears to stand out: studies achieved better success in the overall detection and location problem when using a more adaptable, multi-sensor methodology vice single sensory data acquisition alone [1]. Trends contained in more recent research literature indicate a shift towards multi-sensor fusion and image enhancement techniques. Additional emerging research focuses on post-processing schemes that incorporate machine-learning algorithms in analysis when applied in a broader framework, namely, large datasets. Given the marginal successful indications noted in literature, the overall unifying theme is that the studies focus on

specific dependent variables and environments; resulting in an inability to provide broad IED detection capability for deployment in multiple combat environments.

Accordingly, this research proposes exploring the potential use of infrared (IR) surface images combined with finite element models (FEM) for detection of buried objects in soil.

A. BACKGROUND

This section is intended to serve as a broad overview into potential approaches utilized within remote detection of explosive devices. While by no-means exhausive, this background material aims to solidify an initial framework in understanding some fundamentals behind existing and emerging techniques applied to solving some elements to this overall task. It is well established within the field of explosive detection that biological and chemical based detection schemes apply various methods to detect vapors emitted by compounds contained in explosive material [2]. Sensors applying these methodologies generally require some form of auxiliary detection support when identifying potential targets of interest.

As documentation in [3], the National Research Council (NRC) performed an extensive investigative survey of modern explosive detection strategies that placed strong emphasis upon techniques with potential to extend standoff distances. Applied within a more broad, operational context, Faust et al. [4], uses clarifying terms that better distinguish steps within the overall detection heirachy. Specifically their research categorizes the previously mentioned biological and chemical strategies as “localization” and “confirmation” processes, respectively [4]. This implies a more defined order of precedence in which to frame various detection procedures aimed at improved adequate standoff distance . This indicates an important destinction in how researchers and industry may need to refine their respective approaches to these challenging tasks.

Biological detection involves the use of microorganisms - bees, rats, and dogs - to detect explosives [2]. Chemical detection of explosive vapors can be performed by sophisticated detection schemes such as fluorescent and spectroscopic [2]. All suffer from sampling reliance requiring air or soil samples be taken from within close proximity to

the surroundings of the threat's location; thus, the scope of applying this method does not lend well to solving the operational requirements that are not accounted for in laboratory based testing.

Research techniques investigating the detectability of bulk explosives material housed within IEDs and landmines has limited scope since this technique only identifies bulky explosives, but does not consistently reduce the probability of false alarm [2]. Nuclear Quadrupole Resonance (NQR) analyzes radio frequencies by an active technique which queries the underlying chemical formulation for specific compounds [5]. Another method, neutron interrogation, attempts to identify an explosive's composition by bombarding the soil, surrounding the IED, with neutrons and later analyzing the scattered product [4]. Some explosives can be readily identified using this approach.

Approaches to exploit the acoustic properties of IED casings by introducing sound or seismic waves to the ground, then analyzing the scattered sound, or studying the vibrational effects imparted to the surrounding soil are also under development. Typical measurement instrumentation may include laser Doppler vibrometers, microphones, etc. [5].

More interesting and mature methods are the electromagnetic detection systems that search for change in electromagnetic properties for shallow surface soils caused by the presence of the buried threat [6]. Systems that use ground penetrating radars (GPR) examine radio wave emissions emitted into the ground and analyze the reflected waves. The discontinuities in the dielectric constants at the boundaries between soil and rock causes detectable changes in the electromagnetic field [5]. Depending on the resolution of the system and the sophistication of the signal processing, a visual image of the buried object can be obtained as well as information on the correlation of the detected object with a recorded library. However, those systems are limited when the threat is small or has low metallic content [7].

X-ray backscatter is commonly investigated technique categorized within the electomagentic detection scheme. This technique analyzes patterns in signal reflections that arise from the likelihood that a buried object will have a different density than that of

the soil surrounding it [8]. While the technology is available, it is limited to very shallow objects since the x-ray penetration is very poor if the source strength is limited to safety levels for a person-portable system [9].

Finally, infrared (IR) and hyperspectral systems detect anomalous variation in electromagnetic radiation emissions and/or reflections due to soil characterization as well as the presence of vegetation immediately above the buried threats [10]. This category includes passive and active irradiation techniques and uses a broad range of electromagnetic waves. Within the context of this study, passive detection techniques are preferable for surveillance, so not to alert the adversary to our intentions.

The common characteristic of all methods is complexity and involves high cost, emission from the active system that could give up the location of the operators, heavy signal post-processing and analysis required and high rate of false alarm. Industry and academia are investing resources and time to improve current detection means. The current trend is the quest for simpler, smaller form factor, more efficient, less expensive IED detection/identification means [7]. In this context and given the impending necessity to reduce the vulnerability of the U.S. troops to this deadly threat, the Sensor Research Laboratory (SRL) at the Naval Postgraduate School (NPS) started investigating means to detect buried IEDs using infrared images from commercial IR cameras, to fulfill the interest of the Office of the Naval Research (ONR), which has sponsored this research.

B. THERMAL APPROACHES

Despite the technological gains realized in sensing applications devoted to IED related detection techniques, most approaches documented within surveyed literature are most notably limited by standoff detection. Thermographically themed approaches to this challenging field of study also suffer from this limitation but appear to offer useful insight into aspects of hidden object detection. This section highlights ongoing research efforts among the variety of thermal imaging based approaches devised to resolve this inherently difficult task.

Buried explosives possess thermal diffusivities and heat capacities that differ from the soil, resulting in a detectable variation in soil temperature above the device. In

addition, to temperature variations perceived, comparisons in thermal diffusivities differ among cases exploring undisturbed and disturbed soil by the IED/landmine placement has been shown as a useful technique to determine the probability of detection and identification as summarized by Hibbitts in [6]. Detection of a buried explosive via infrared techniques primarily relies on the variation of thermal characteristics between the soil, above the device, and that of the surrounding environment.

Much research has gravitated towards the investigating of IED emplacement indicators which is well documented in [8]. Indications in related research presented by Simunek et al. [11] focused special attention to the surrounding soil's characterization. In another study led by Hibbitts and research associates [6], soil disruption effects associated with emplacement activities (digging, soil layer mixing, burial) identified thermal constrasts relating optical properties (soil) with the surrounding soil's measurable thermal properties. This interpretation, requiring significant in-depth of specific soil properties, is widely held in literature utilizing thermographic detection schemes. Simunek further details soil composition parameters including size distribution, grain shape, surface roughness and topography as having impact to detectable temperature variation. The dynamics governing the reversal rate of these properties to original surface conditions after an object has been buried substantiates experiments citing observed diurnal phenomena [10]. The link between this time dependent effect (diurnal) and disturbed soils is not widely understood [10].

Specific characteristics of the soil surface, such as granularity, compactness, water content, topography, depending on exposure of soil to solar radiation, weather conditions and temperature are represented uniquely based on the device's spectral range infrared band that captured the imaged scene [12]. For each time of the day or night a particular emphasis in specific characteristics can be observed differently depending on the spectral range [13]. Their combination (data fusion) allows the enhancement on the contrasts between the soil atop the buried device and its surroundings [11]. We intended to explore those differences to develop a method of detection and identification that combines images in the spectral bands previously described.

Several previous reports detailed experimental work characterizing this difference when applied under field-testing conditions. Bowman et al. [14] and DePersia et al. [15] reported the main results from the DARPA Hyperspectral Mine Detection program (1994-1999), which examined hyperspectral sensors for standoff mine identification. They reported two main scenarios where temperature variation maybe used as a detection technique. For recently buried mines, the disturbed soil is typically less dense and compacted, resulting in a lower thermal conductivity and thus a higher temperature. As noted by van Dam et al. [16], weather effects quickly eliminate this soil effect, but a temperature variation can still be observed for devices buried given a longer duration of time. These observed differences are described between the measured quantities attributed to the explosive's thermal diffusivity and soil's heat capacity [16]. A challenge with this identification approach; however, is the variation in the temperature anomaly when taken collectively with other thermal effects. The diurnal heating/cooling cycle, the moisture content of the soil, and false positives from other thermal objects (such as subsurface rocks) were also found to complicate the identification of a buried explosive with LWIR. Simard [17] summarizes a range of experimental mine detection via IR cameras in the early 1990s, and also proposes two simple analytical models to account for the diurnal variation in the absence of the soil effect mentioned previously [16].

Considerable recent work on IR imaging of buried explosives has been sponsored by the U.S. Army and the Night Vision and Electronic Sensors Directorate which are cited frequently in numerous conference papers. Forward-looking IR devices have been tested in a variety of field conditions and are frequently combined with ground-penetrating radar (GPR) or other detection schemes for multispectral analysis. Hong and coworkers [18] report spatial and temporal variation of soil temperatures for IR imaging based on testing at New Mexico Tech and the Netherlands Organization for Applied Scientific Research (TNO). Stone and coworkers at the University of Missouri have performed a range of IR imaging studies and algorithm development for the Army Research Office, including sensor fusion with GPR [13]. They also examine numerous image processing techniques and algorithms for background/anomaly discrimination in attempts to better explain diurnal variation observed. Cremer and coauthors [19] report

similar work on vehicle mounted IR cameras for mine detection at TNO, with an emphasis on image processing algorithms and comparison of camera mountings.

The common characteristic of the previous works analyzed indicate in-depth knowledge requirement of some soil characteristic or overall characterization. This has lead to limited levels of success.

C. RESEARCH OBJECTIVES

Recently, researchers from the Sensor Research Lab at NPS started to investigate means to detect shallowly buried objects using infrared surface images. This project was driven by the need to find an alternative and simpler approach to detect potential threats such IEDs and landmines. In this context, the objective of this research is exploring the potential use of infrared surface images combined with finite element models for detection of buried objects in soil.

To achieve this goal, infrared surface images are generated, post-processed and combined with finite element modeling and simulation to support the investigation of the circumstances of detection and identification of buried objects that pose threats, such as IEDs and landmines. With this study, we intend to answer the following research questions:

1. Is it possible to estimate the size, shape, and/or pattern of the buried IED or landmine using surface images taken in long-wave (LWIR), mid-wave infrared (MWIR) or near infrared (NIR)?

2. Is it possible to obtain a volumetric insight of the buried object using only surface images of one or more IR bands?

3. How does the burial depth affect detection/identification? What are the conditions and limitations?

4. How does the material, volume, size, and shape of the buried object affect detection/identification?

The effort to answer these questions is made under the assumption that detection of a buried object via infrared sensory depends on variation of thermal characteristics between the soil above the device and that of the surrounding environment. This translates into the contrast between the regions on the surface temperature images whose influences we seek [1], [20].

Different thermal sensors present the opportunity to capture different scene details. If the representative IR images from different bands are fused into a composite image, applying image enhancement techniques filters noise and other undesired things that obstruct. In addition to possibly revealing a buried object's location, we might have a means of classifying it and thereby reducing false positives. Hopefully, a focused analysis of altered optical properties of the surface will link residual effects of emplacement activities with weather effects and the composition of a buried target with respect to its surroundings [1], [20].

D. THESIS ORGANIZATION

This thesis is organized as follows: Chapter I has discussed the motivation behind this project and provides a brief synopsis on alternative approaches attempted within the scope of remote detection of buried energetics. Chapter II presents the design considerations and sampling of various run-time configurations used in the Finite Element Model (FEM) simulations and subsequently implemented by Multiphysics software, COMSOL. Chapter III describes the experimental range assembled to collect the images from the infrared cameras and the post-processing performed to identify the component elements that compose a buried object's thermal signature on the images to enhance probability of detection.

Results presented in Chapter IV examine the benefits from the combination of FE simulation and infrared image sets evaluated within the context of this study. Research questions presented in Chapter I, Section C are answered. The final chapter summarizes the project and provides suggestions for improving and continuing this research.

II. DESIGN CONSIDERATIONS FOR FEM

The previous chapter presented an overview of varying methodologies applied in the study of detection and localization of buried IEDs. Background and research objectives establish baseline reference within literature regarding passive IR capability and focus for this study. This chapter describes how the FEMs proposed within the context of this study have promoted understanding encapsulating buried object detectability. Applying insights gathered through the course of this study assisted in refining some assumptions made in initial modeling efforts. Chapter III discusses some of these to include the experimental setup and data acquisition implementations.

The development and application of FEMs in the scope of our investigation simplified problem complexity with respect to perceived parameter coupling. Moreover, with knowledge of material properties (IED and soil), it is possible to estimate the absolute temperatures of the bare soil and the soil atop the buried sample. This allows for determination of the required sensitivity of the IR cameras. Note that the thermal properties of soil and IEDs can be very similar, as shown in Figure 1. For example, sand/ Teflon possess similar characteristics of soil/IED found in actual scenarios, imposing challenges for the detection scheme.

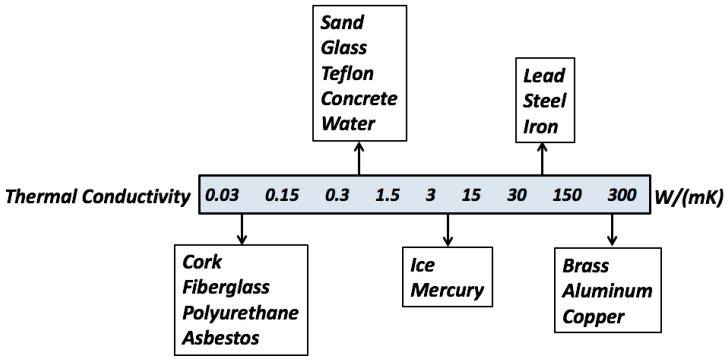

Thermal conductivity of several materials, used to compare with the conductivity of sand, soil chosen to be used in this study.

Figure 1. Thermal conductivity of common materials

A. FINITE ELEMENT MODELING

Models constructed and later utilized in simulation scenarios were originally generated using COMSOL Multiphysics, a robust software application, which allows the incorporation of multiple phenomena in the same simulation scenario. For modeling the detection of a buried object, we envisioned the experimental setup and tried to recreate the same conditions. Therefore, a box containing the soil (sand), buried sensors and IED emulator was placed on a concrete floor with the cameras pointing to the region of interest. Figure 2 shows the schematic diagram of the model geometry.

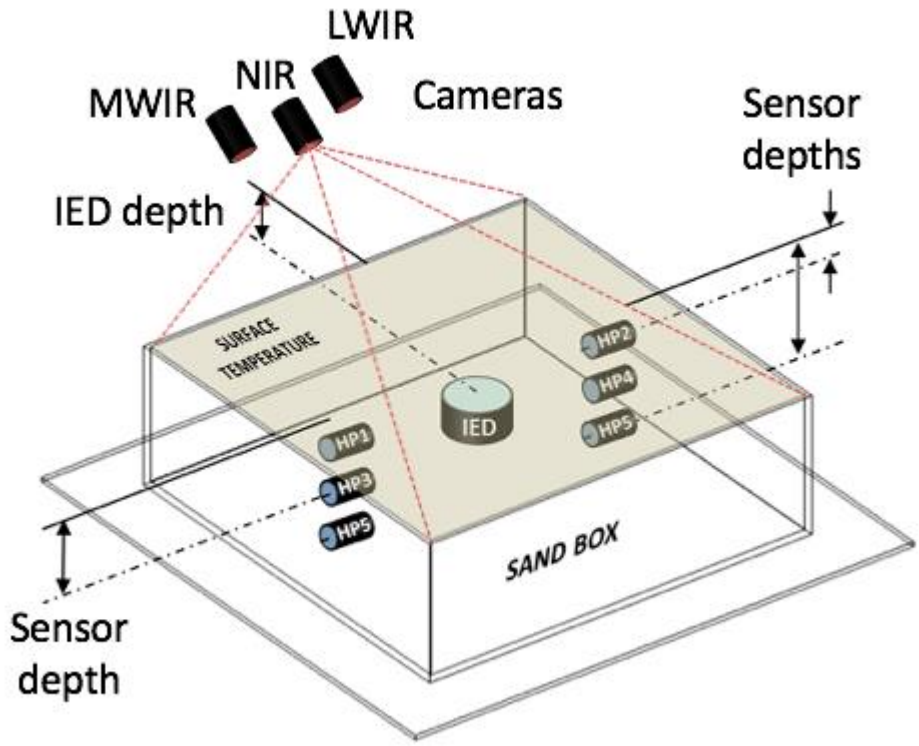

Schematic geometrically depicts sensor placement in relation to a buried object's location. Red dashed lines mark fixed camera array's field of view. The tan region, composed of sand, denotes the planar surface temperature map detected by one or more IR cameras. The sand box enclosure contains the buried object (IED) and soil sensor set (cylinder). Concrete plane lies below enclosure's wooden base.

Figure 2. COMSOL-generated representation depicting key FEM components' relative spatial distribution

1. Environment

To enable relevant equations for computation involving heat transfer, we created boundary conditions within COMSOL's interface and applied these constraints per our model's specifications. Doing so allowed our model to incorporate a range of heat transfer dynamics including conduction, convection, radiation, and surface-to-surface radiation. Enabling this interface incorporates external radiance and ultimately impacts the buried energetics' temperature profile over time computed. This source boundary condition was applied to domains which might be exposed to sunlight. In the context of our simulation, the external irradiance (due to sun) parameter used was approximately 900 (W/m^2), when no such information was available, which was subject to further constraint by the geographic location, season, and time of day. Additional ambient settings values defined included ambient temperature (T_{amb}) of 293.15 K, and absolute pressure (p_{amb}) of 1 (atm).

2. Buried Device Attributes

To better understand the interactions between the buried device and its surroundings, relevant dimensional and material properties were defined for use in parametric sweeps on the model. Buried device attributes at the focus of our study included diameter, radius, height, and burial depth. Among the material properties, thermal conductivity (*k)*, which accounts for the buried device's ability to absorb and dissipate heat, was parameterized for the initial simulations. Boundary conditions for the experimental setup with respect to the enclosure's material composition and dimensions were parameterized so that we could observe any impact on the buried device's thermal profile and overall impact to the model's fidelity.

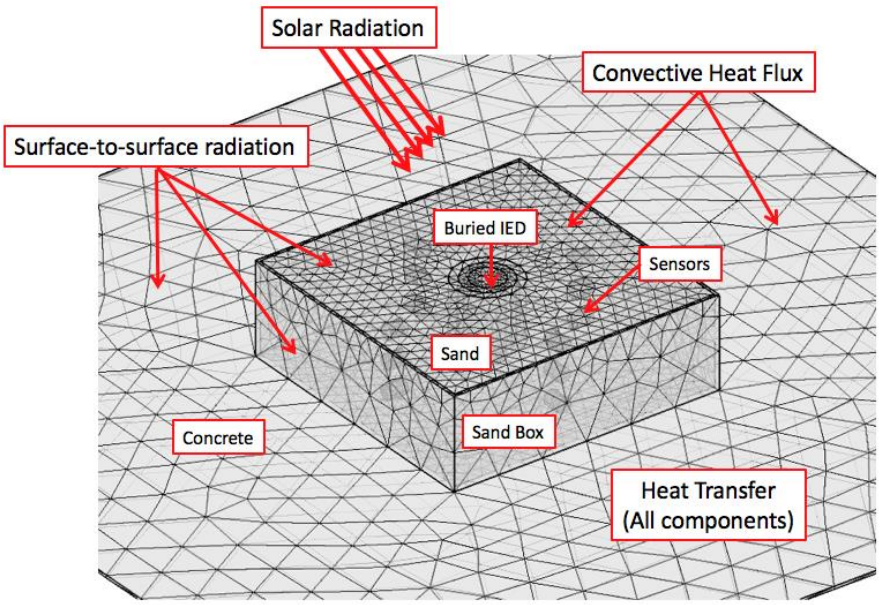

Figure 3. COMSOL-generated diagram depicting experimental setup to obtain surface temperature maps of sand.

The solar radiation was introduced to simulate the diurnal conditions of Monterey during summer time. In addition to time of day, COMSOL enables setting the geographic coordinates and time of the year within the model. This accounts for variation in the solar radiation direction and intensity based on time and location.

One great advantage of this model is the ability to eliminate boundaries such as the box and concrete to simulate the IED buried in an open area (more realistic situation) and then include the boundaries to simulate the actual experimental setup and understand the impact of those boundaries on the detection.

B. IMPLEMENTED SIMULATIONS

The ultimate goal is to find a transformation that allows for extrapolation of the results obtained on a confined space (experimental setup) to be applied to a more realistic setting such as an open field. The following figures show the simulation performed on this condition, for several varying parameters. The dependent variable is the difference in the surface temperature between the soil layer above the IED and its surroundings (ΔT), in Kelvin. This was performed by taking the average surface temperature in a couple of

squared boxes between the center and the edge of the box, representing the temperature of the surroundings and taking the average surface temperature of a square box in the center of the box, representing the soil layer above the IED.

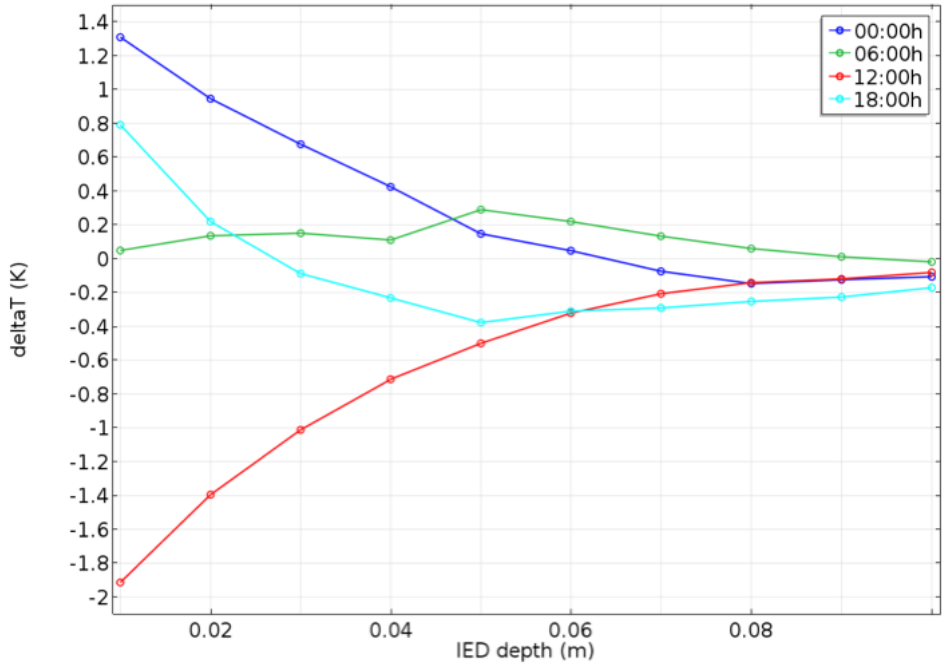

Data taken 4 times daily over a period of 1 day. IED specifications: material—Teflon, diameter—8 inches, height—4 inches.

Figure 4. Impact of IED depth on temperature of soil surrounding IED

As depicted in Figure 4, ΔT decreases as the burial depth increases. The rates are different depending on the time of the day and the boundary conditions imposed such as ambient temperature, solar radiation, wind, etc. Notice that at 6:00 AM, ΔT is very small and remains almost unchanged with depth. Figure 5 shows how ΔT changes with the material thermal conductivity as all other properties remain unchanged.

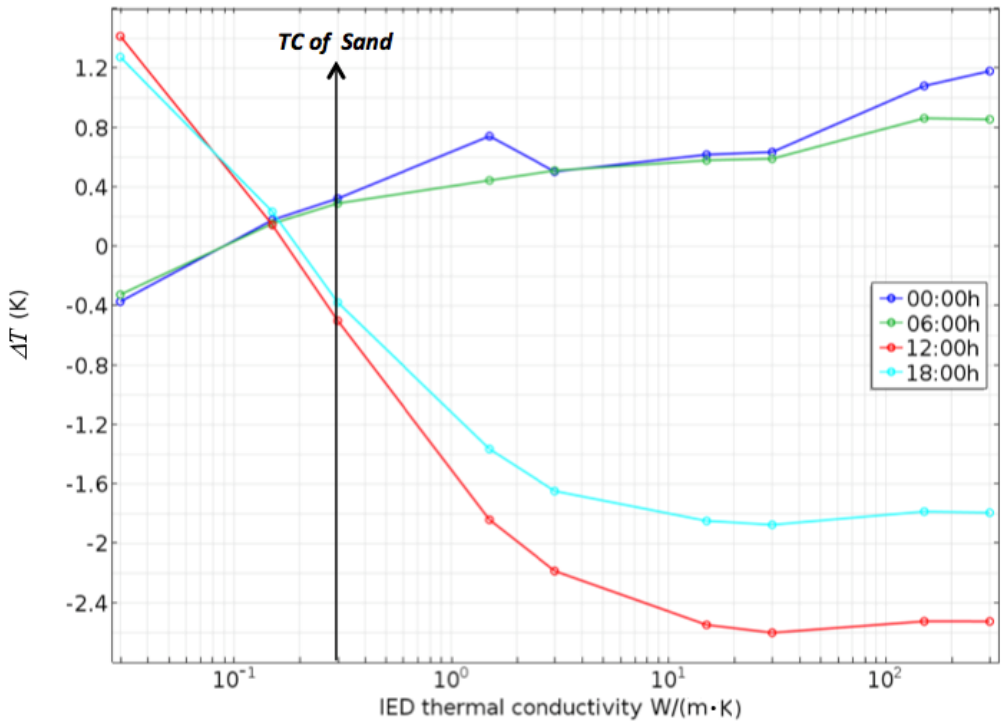

Data taken 4 times daily over a period of 1 day. IED specifications: burial depth—2 inches, diameter—8 inches, height—4 inches.

Figure 5. Impact of IED material on temperature of soil layer above IED and its surroundings

It is clear that ΔT increases as the difference between thermal conductivities, soil and IED respectively, increases. It also can be observed that there is an inversion in ΔT when the thermal conductivity of the buried object is lower than that of the soil. This is expected as the heat transfer dynamics change at the analyzed volume. Another interesting observation is the saturation of ΔT beyond 30 W/(m·K) that happens at the times of day where the IED is colder than the surrounding soil (12:00 and 18:00). This result indicates that materials with thermal conductivity in the saturation region, such as aluminum, brass, steel, iron, copper, etc., cannot be distinguished by this property.

Figure 6 shows how ΔT changes when the volume of the buried object changes while the surface area remains the same (see diagram on left side of the figure). For all selected times of the day, ΔT remains almost constant.

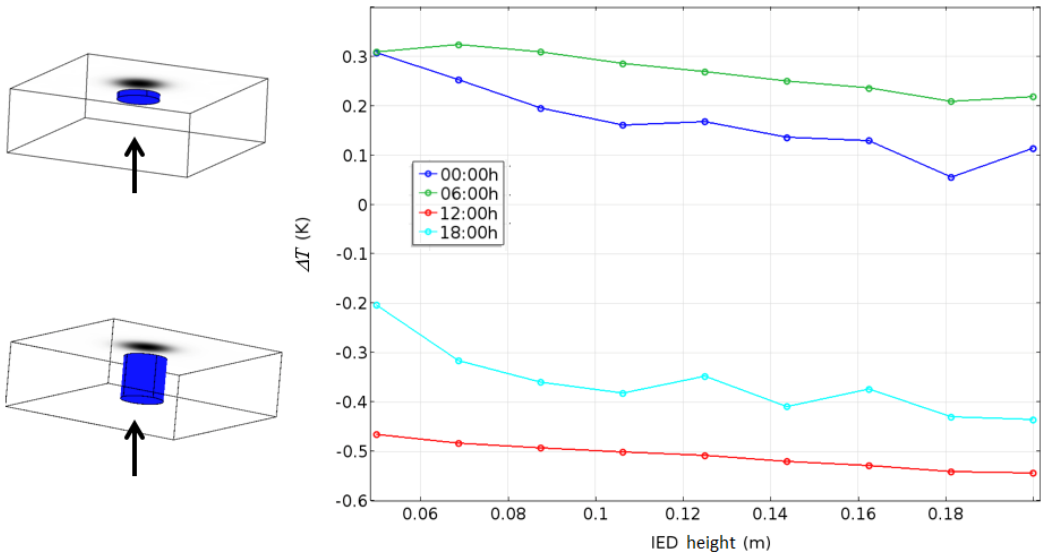

Data taken 4 times daily over a period of 1 day. IED specifications: material—Teflon, burial depth—2 inches, diameter—8 inches.

Figure 6. Impact of IED volume on temperature of soil layer above IED and its surroundings

For the case where the surface area changes, ΔT increases more prominently for the times of the day where the IED is colder than the surrounding soil (12:00 and 18:00), as shown in Figure 7. The size of the thermal anomaly is greatly affected when the orientation of the buried object is changed (see left side of the figure).

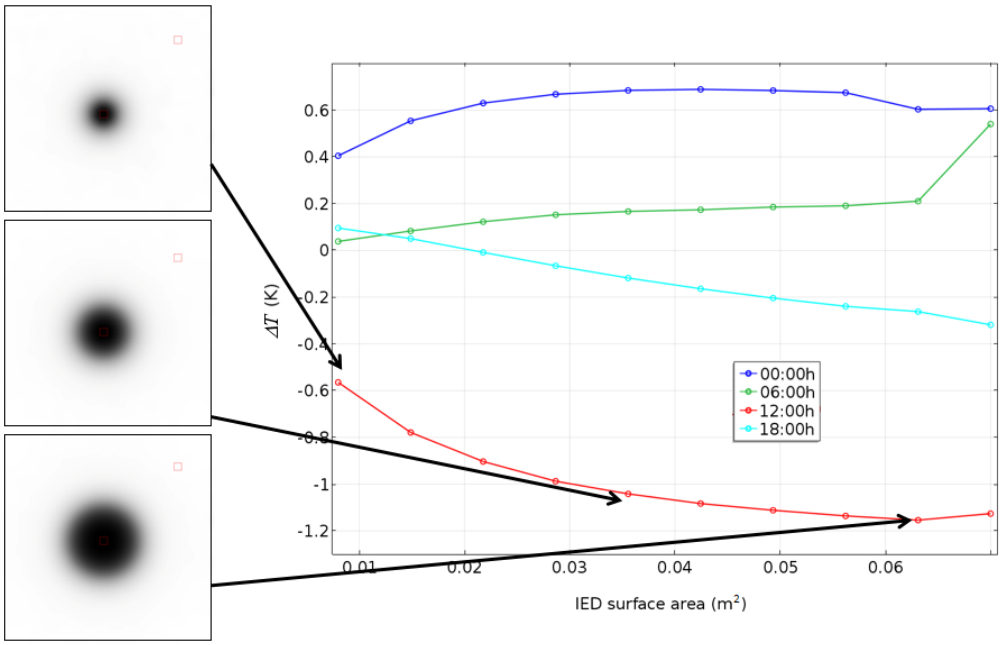

Data taken 4 times daily over a period of 1 day. IED specifications: material—Teflon, burial depth—2 inches, height—4 inches.

Figure 7. Impact of IED surface area on temperature of soil layer above IED and its surroundings

Figure 8 shows an example of the noticeable change in the thermal anomaly shape with burial depth. As the triangular object is buried deeper and deeper, the thermal anomaly shape starts to blur and loses its sharpness. This makes the shape identification difficult beyond certain depths.

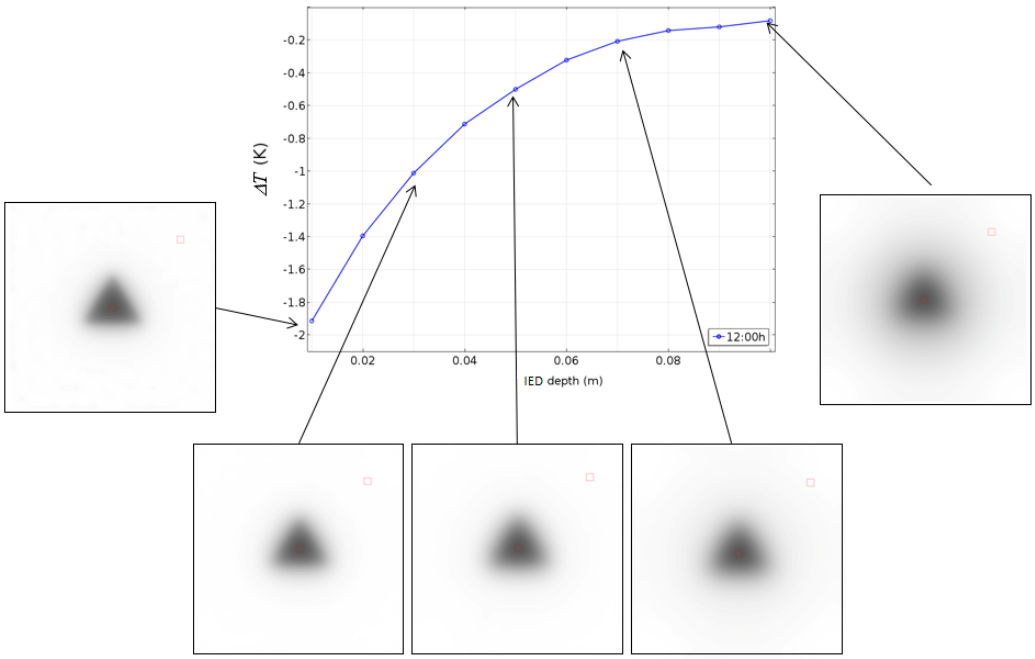

Data taken 4 times daily over a period of 1 day. IED specifications: material—Teflon, shape—triangle, burial depth—2 inches, side length—10 inches.

Figure 8. Impact of IED shape on temperature of soil layer above IED and its surroundings

Lastly, Figure 9 shows the result of a simulation when we consider the disturbed soil atop the buried object. This was performed by keeping all other properties fixed and changing the density of the sand, which is the predominant source of impact on ΔT as we will discuss in a later section.

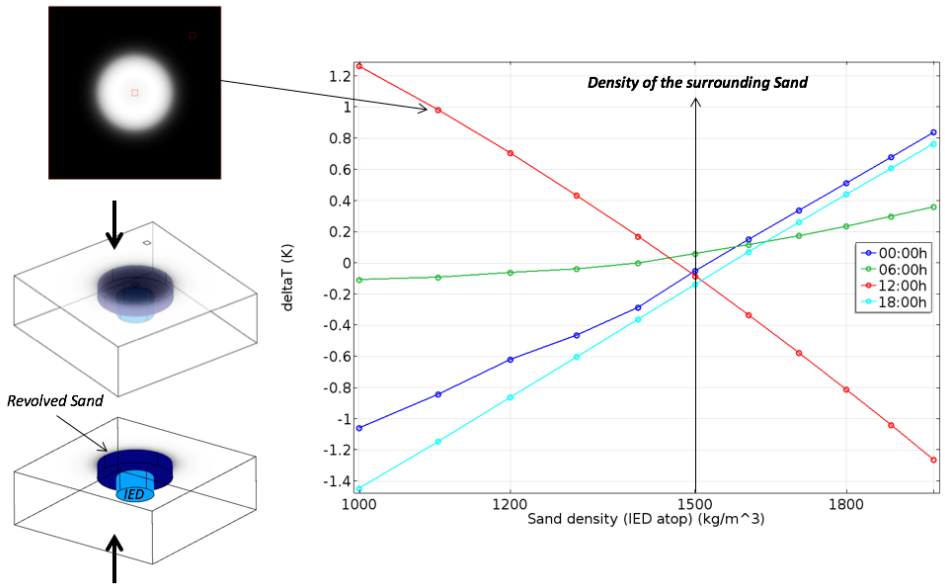

Data taken 4 times daily over a period of 1 day. IED specifications: material—Teflon, burial depth—2 inches, diameter—8 inches.

Figure 9. Impact of soil scarring (density) on temperature of soil layer above IED and its surroundings

It can be observed in Figure 9 that there is an inversion in ΔT at the point where the density of the sand layer above the IED matches the surrounding soil. The left side implies that the disturbed soil is less compacted than the undisturbed area whereas the right side of the graph implies that the soil was compacted, probably for deception reasons, resulting in a higher soil density than the undisturbed area. In both cases there is an enhancement in ΔT.

This analysis is far from comprehensive and many strong constraints were made for the sake of simplicity; however, it shows that the FEM provides a reasonable way to obtain insights on what to expect for the actual measurements and to understand the impact of several parameters on the detectability of the buried object. The simulations performed thus far considered the parameters were uncoupled, which is a great simplification. Although our simulations utilized this simplification, FEM can be used to analyze coupled parameters using some deconvolution techniques, which we suggest be addressed in future work.

III. EXPERIMENTAL RANGE

Building upon the methodology described in the previous chapter, this chapter describes the details governing the physical experimentation and data collection process.

A. EXPERIMENT DESIGN AND SETUP

To validate the model utilized in the simulation and to reduce overall problem complexity, we elected to use a controlled soil, to eliminate surface clutter, and to record measurements under environmentally ideal conditions. Overall, the design is flexible and allows for incremental introduction of other environmental effects and is open for future research.

The experimental setup, shown in Figure 10, currently consists of a 36-inch square sandbox with aluminum-covered sides and a wooden frame. The experiment collects data through an array of sensors that allow for the area in question of the sand box to be measured, including the surrounding conditions for future extrapolation and error analysis. The sensory array is a combination of a weather station, buried soil sensors, and three infrared cameras (LWIR, MWIR and NIR).

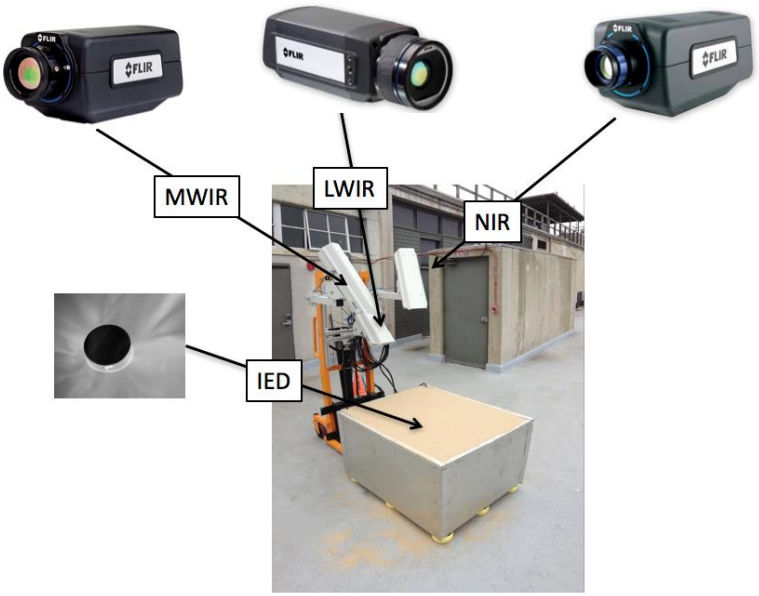

Figure 10. Photo of experimental setup with infrared cameras; weather station and buried sensors not visible

Since weather conditions impact the thermal factors measured and ultimately correlate with the resulting images, the experimental setup considers weather related measurements. Using an Onset HOBO Weather Station setup, measurements captured data for solar radiation, wind speed, air temperature, and humidity. Specifically, solar radiation measured with a silicon pyranometer sensor reports ±5% accuracy and 1.25 W/ m^2 resolution; wind speed is measured with ±4% accuracy and 0.5 m/s resolution; air temperature and humidity are measured with a single solar radiation protected sensor with accuracy of ±0.21ºC and ±2.5% and resolution of 0.02 ºC and 0.1% RH.

Preliminary infrared images show a direct correlation between the buried object and its ability to absorb and dissipate thermal energy into its surroundings. To better understand the solar heating cycle throughout the day, a set of buried sensors were used to monitor the parameters of soil temperature and moisture content. Initial infrared images and soil parameters measured by the buried sensors show the effects of solar heating on the sand. Our investigation focuses on the heat balance of the IED's surroundings as well as the effects of the heat's influence upon controlled boundaries.

To account for the impact soil moisture may levy upon a buried object's thermal signature, soil sensors recorded this related data from varying depths. The soil sensors used are a set of 6 Stevens HydraProbe II buried at three different depths, as depicted in Figure 11, on both sides of the sandbox. These sensors measure many different properties in the sand, with soil moisture and temperature being primary data collected for this experiment. They have an accuracy of ±0.01 WFV and ±2.0% respectively. Recorded soil sensor data in combination with the weather station gives pertinent information on the conditions surrounding the buried object. This allows for correlations and analysis to be made when observing different buried objects in different conditions.

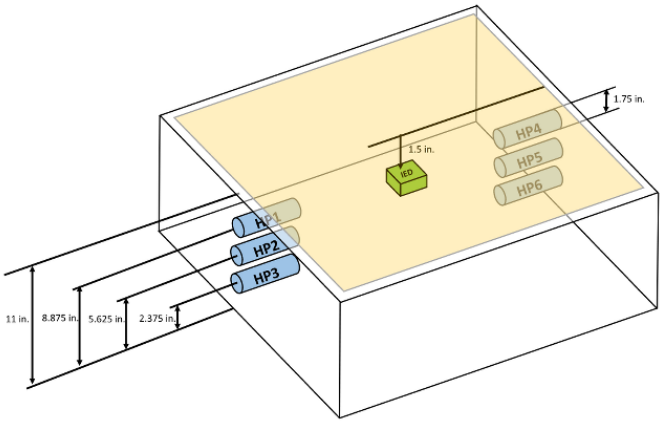

Figure 11. Diagram of experimental setup depicting position of sensors and buried Teflon object in sandbox

A set of three thermal infrared cameras optically surveyed the experiment and recorded the thermal response within each camera's respective operational range. The infrared cameras are mounted between 1 and 2 meters from the surface to keep the field of view around 4 inches inside the sandbox. The LWIR camera is a forward-looking infrared (FLIR) A655sc with a spectral range of 7.5 - 14.0 μm, a resolution of 640 x 480 pixels, temperature accuracy of ±2%, and Noise Equivalent Temperature Difference (NETD) of <30 mK. The FLIR A6750sc has a spectral range of 3 - 5 μm, resolution of 640 x 512 pixels, temperature accuracy of ±2%, and a NETD of 18mK. The NIR camera is a FLIR A6251sc with a spectral range of 0.9 - 1.7 μm, a resolution of 640 x 512 pixels,

and quantum efficiency of >80%. These give reasonable resolution and operational outputs to measure and observe their respective ranged on all three atmospheric windows of the infrared band.

B. DATA COLLECTION

Images and data collected was subjected to minimal pre-processing and cataloging procedures using a computer running HOBOware and LabVIEW. HOBOware is Onset's software used to interact with the weather station and was used only to retrieve the data stored on the station and reset the settings. Weather data was tabularized and combined with other collected data. LabVIEW is a visual programming interface that allows for parallel processing and acquisition from a large array of sensors and other devices.

Jeffrey Catterlin, a SNR team member, developed a program specifically for this project to collect images and data from the cameras, as well as collect data from the buried sensors. The program performed these tasks: read the per pixel temperatures readings from the IR cameras, analyzed up to 5 designated regions of interest in this image, as shown in Figure 12, recorded the minimum, maximum, and average temperature for the regions, and placed them alongside the contrast enhanced image with the minimum and maximum image temperature. Finally, the program saved a set of data from each of the 6 buried sensors. Also, the NIR camera's images were contrast enhanced and recorded including the integration time and frame rate.

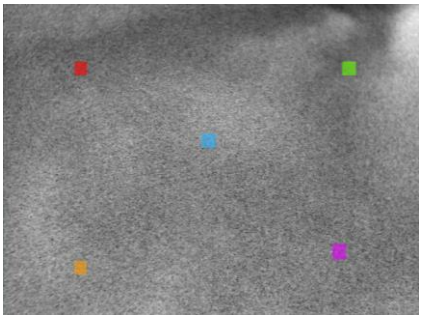

Red, green, orange, and magenta markers are edge samples. Center blue marker indicates relative location of the buried IED emulator, which is hidden by a layer of soil in the LWIR image.

Figure 12. LWIR image with designated regions of interest marked

This setup allowed for large amounts of flexibility for measuring and analyzing data as all relevant data was saved as a series of tables that can be compiled together using MATLAB or other data analysis tools. Additionally, the current experimental data collection scheme allows for future upgrade and the addition of further features. This includes addition of image processing and any feature that needs to be performed in real time.

A planned future modification is to use a hole in the ground filled with controlled soil instead of a sandbox. This will give more realistic boundary conditions by having true soil on the edges and reduce the influence of cooling and heating from the side of the box since the sides will be eliminated. The ground will also provide a more realistic drainage and water level compared to the current experimental setup.

C. DATA PROCESSING TO ENHANCE PROBABILITY OF DETECTION

Although the experimental range incorporated three infrared bands, only the LWIR images were used in this work. Future efforts will benefit from the other data sets.

1. Direct Image Processing

Once sand surface images were acquired, it was necessary to run a feature extraction routine to explicit a particular shape or topology information related to the presence of the buried sample. Ideally, this routine should be based on transformations of the raw image capable of enhancing contrasts, correcting eventual lighting non-

uniformities, detecting the image background and performing a threshold operation that turns evident the effect of the buried object on the sand surface region directly atop of it.

Within existing literature were very well-established image processing operations and software packages that perform these operations. The first approach used built-in operations from MATLAB Image Processing Toolbox to address feature enhancing and detection from the buried object scene on each single-band IR image. The images were loaded into MATLAB and, from that point forward, treated as matrices, where the row, column indices (i,j) were used in direct correspondence with the geometric position of the pixels, with the origin placed at the top-left corner. The matrix elements' values represent pixel intensities, which in turn, correlates to scene radiance (or temperature). The aforementioned transformations were performed in a linear algebra sense and translated into matrix operations for utilization in MATLAB.

Image observation over a day period allowed observation that the image background switched from a dark background during the nighttime to a bright background during daylight hours. Concerning the buried object and its observed effects on the surface radiance (or temperature), it was also observed a cycling action from brighter (hotter than the surroundings) to darker (colder than the surroundings), respectively. Also, during the same daytime (night or day), the matrices average values (average pixel value) varied, indicating a background average intensity variation. In general, the algorithm utilized should first detect whether the image contains a bright or dark background and then try to equalize pixel average values before going into any feature detection; that must assume a threshold value for disturbance detection. The convention the Find Feature algorithm utilized was of a dark background; therefore, when a bright background was detected, it was converted to a dark background through a negative operation. From this point forward, both kind of images were treated the same way. Figure 13 shows a schematic diagram of the algorithm employed.

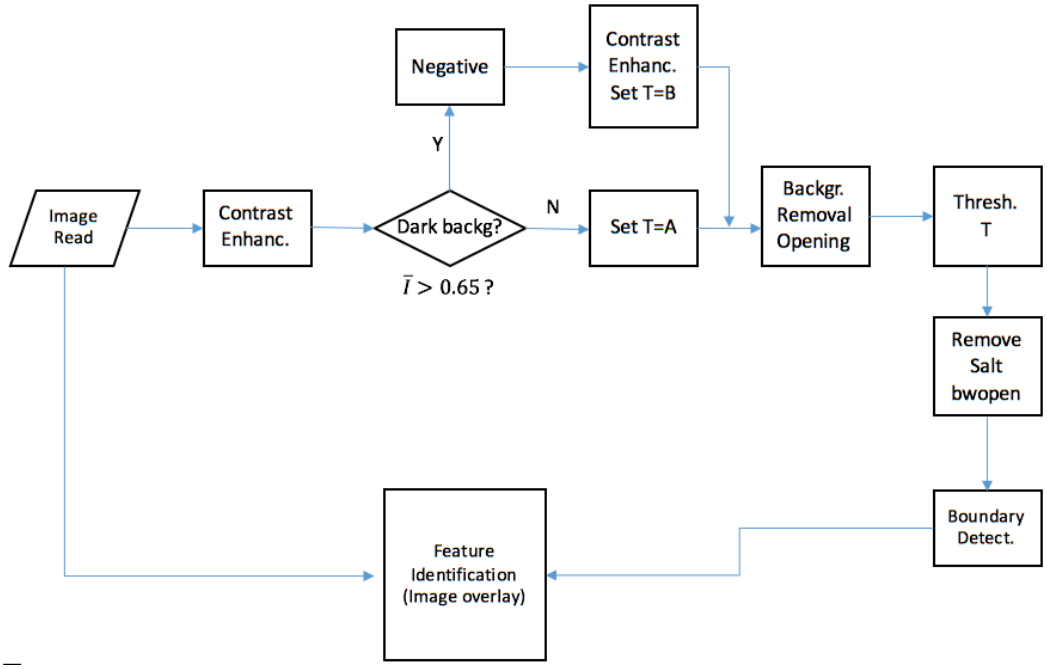

Figure 13. Schematic diagram of the image processing algorithm workflow

The approach of feature-processing dark background images was chosen due to its intuitive appeal that thresholding an image with the desired feature of detection exhibiting a higher intensity than its surroundings yields a processed image with the feature on a high logical level (white) against a background on a low logical level (black). Some LWIR images with the overlaid feature contour obtained with the routine above are presented on Figure 14. In the images presented, the desired features were detected, and their contours were highlighted in green.

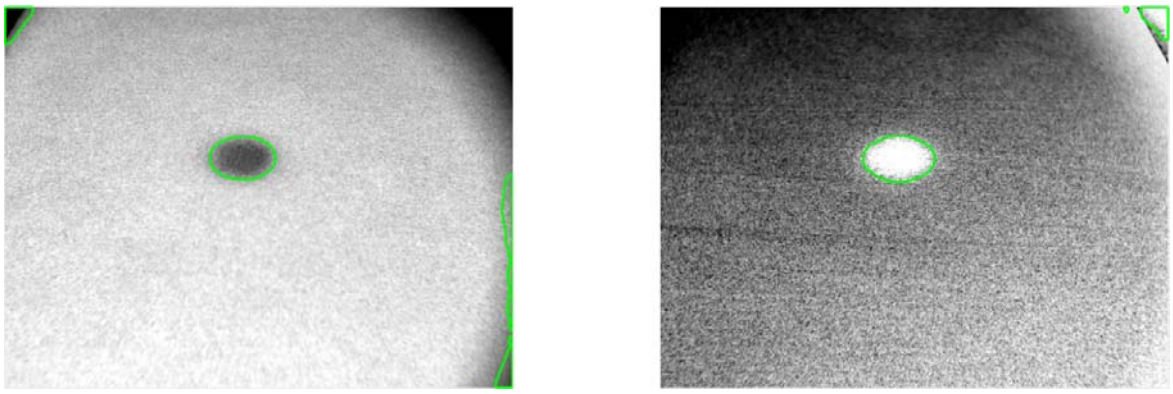

(a) (b)

(a) Detected feature contour (green) overlaid on a bright background image taken at 12:00 09/01/2017; (b) Detected feature contour (green) overlaid on a dark background image taken at 18:00 08/31/2017.

Figure 14. Sample images processed with the Find Feature algorithm

Although the implemented algorithm was capable of correctly detecting the buried object on the images shown in Figure 14, its efficiency at different times of the day, hence with different contrast ratios, was very dependent on the threshold level setting and required a human interpreter to slightly adjust them in between processing. Also, the Find Feature algorithm implemented up to this point did not produce a way of enabling quantitative comparisons between feature detections for the same burial depths at different times of the day or for different burial depths. Consequently, a metric, explicitly the definition of a uniform way of quantifying detection parameters and results for different experimental conditions became imperative. Otherwise, estimating detection probabilities and comparing feature detection in images at different conditions would not produce logical results.

2. Detection Metric

Considering the buried object detection an outlier detection on a larger background hints at a statistical way of treating the problem. Moreover, under the signal processing perspective detecting a feature always must deal with detection limits and contrasts, in which the detection lower limits are almost always defined in terms of a ratio of minimum detectable signal power (or S) with respect to total undesirable power within

the detection bandwidth, or noise power (or N). That ratio is widely known as the signal-to-noise ratio (or S/N). These quantities are always considered and treated statistically. With that in mind, if we consider all the acquired images as statistical entities, it is possible to associate and average the value and a standard deviation of pixel values. Furthermore, if one normalizes each image with respect to its respective parameters (average and standard deviation) in a way that every pixel value will now be transformed into a new pixel value that expresses the number of standard deviations from the image average, it will automatically establish a way of defining what is an outlier, associate a detection probability (assuming a chosen probability density function) and also a way of comparing detection "scores" for dissimilar experimental conditions (time of the day or burial depth).

It is convenient to point out at this point that this approach is valid only if the feature extension may be neglected with respect to the imaged extension, otherwise the image statistics would be disturbed by the presence of the outlier. In cases that this hypothesis cannot be assumed, the statistical properties of the background will have to be estimated based on other observations.

Now, consider the previously located buried object after running the *Find Feature* algorithm included in the Appendix. Following, as a way of showing the process and empirically demonstrating its usefulness, is a step-by-step presentation of the application of this metric for an actual image. Instead of showing bi-dimensional plots, a horizontal line of the raw image (before contrast adjustment), associated with Figure 7 (b), through the center of the detected feature is considered.

The corresponding line, extracted from the acquired raw image (matrix row) centered with respect to the sample, is plotted in Figure 8. It is worth noticing that the image is spatially sampled with pixel spatial resolution (horizontal axis), while the vertical axis (temperature) is quantized with 16 bits. Next, the selected line is extracted not from the raw image itself, but from an image file processed in the way proposed for the detection metric, say subtracting, from every pixel value in the image, the image average intensity (μ) and dividing the result by the image intensity standard deviation (σ), explicitly:

$$\overline{I_{ij}} = \frac{I_{ij} - \mu}{\sigma} \tag{1}$$

where $\overline{I_{ij}}$ is the transformed intensity of the pixel located at image coordinates (i, j), I_{ij} is the intensity of the pixel located at the same coordinates on the acquired raw image.

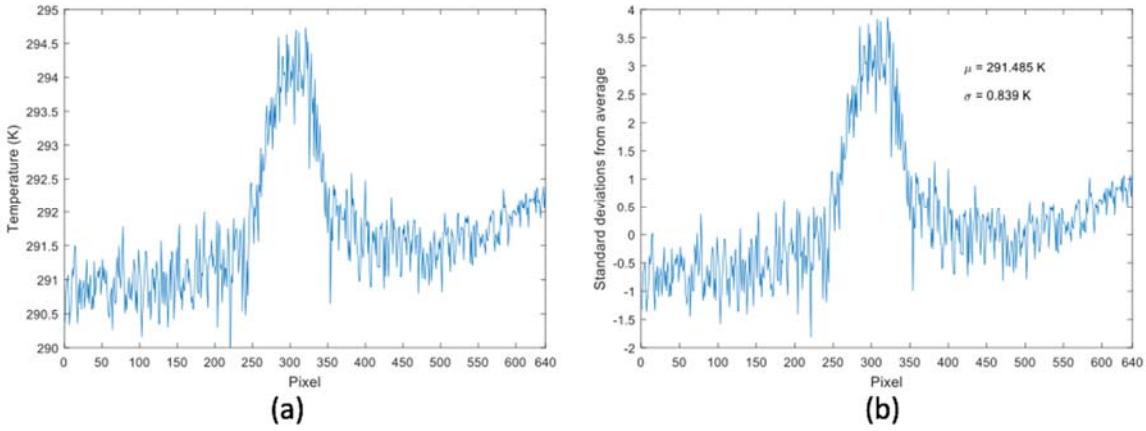

(a) Image line extracted from temperature file. (b) Line extracted from the transformed image through the use of the detection metric expression.

Figure 15. Comparison of actual image line and transformed image line

The plot of the same selected line extracted from the image obtained after the transformation just mentioned is shown in Figure 16. The average and standard deviation shown are obtained from the whole image. Their values are printed along with the plot. A further improvement of the metric is performed using the root-squared value of the previously calculated value to avoid negative values and also make the metric insensitive to image polarity (dark or bright background), explicitly

$$\overline{I_{ij}} = \sqrt{\left(\frac{I_{ij} - \mu}{\sigma}\right)^2} \tag{2}$$

The results from this approach for the two images in Figure 4 are presented in Figure 7 in their respective positions.

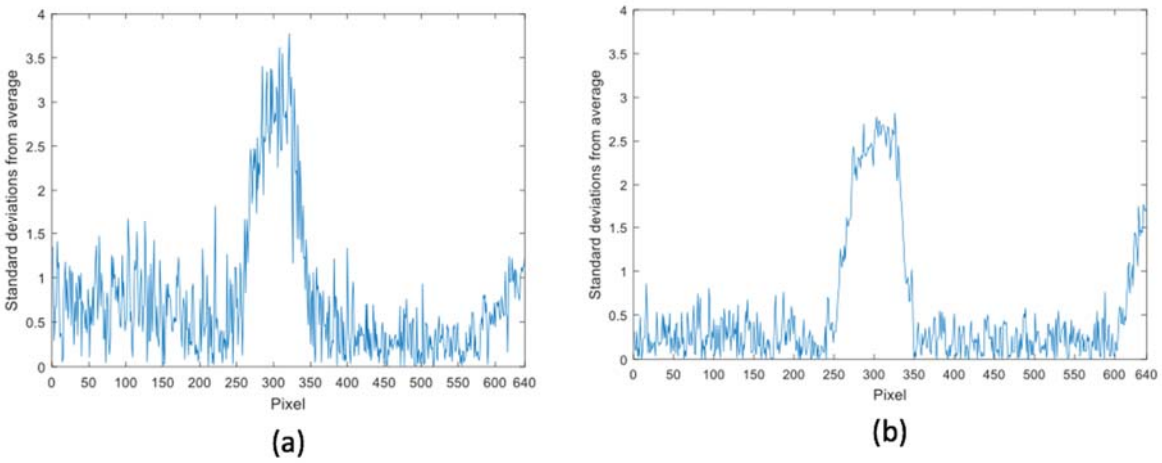

(a) Image acquired at 12:00 09/01/2017; (b) image acquired at 18:00 08/31/2017.

Figure 16. Line from transformed images associated with Figure 4 through use of modified detection metric (root-squared)

Figure 16 demonstrates that the contrast is still high as expected and the values are all non-negatives. This signifies that image polarity plays no role in the transformed image although the low-light image is clearly noisier.

THIS PAGE INTENTIONALLY LEFT BLANK

IV. RESULTS

Preliminary LWIR raw images show that it is possible to detect buried objects. Figure 17 shows the comparison between the difference of the average surface temperatures atop a buried Teflon object at 3 cm from the surface and its surroundings, extracted from the LWIR images and that estimated by the thermal transport model. The data corresponds to a period of nine consecutive days recorded in a range located in Monterey, CA, in September 2015. These results show that passive LWIR detection of a buried object is easier when temperatures are close to the maxima and minima. Furthermore, the difference is accentuated in the daytime when the temperatures are in the highest levels, as shown in Figure 17.

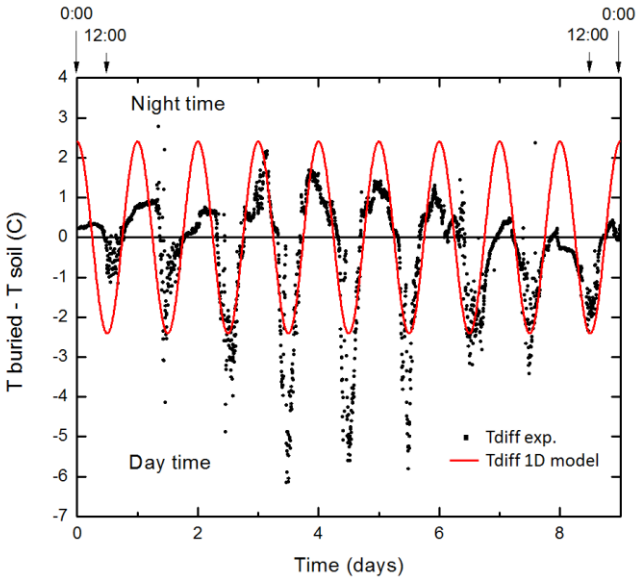

Teflon sample buried at 3 cm from the sand surface, extracted from the raw images, and data estimated by a 1D thermal transport model, to guide the eye.

Figure 17. Comparison of temperature difference between soil above sample and soil surrounding sample

Since the analytical model does not account for thermal properties dependence on temperature and the ambient temperature is considered fixed for the entire period, there is a clear discrepancy between day and night time values. This is corrected in FEMs as can be seen in Figure 4. In addition, it can be observed in Figure 18 how the depth of the buried object affects the maxima and minima of ΔT along the time of the day. The deeper the object the later in the day/night the minima/maxima will occur.

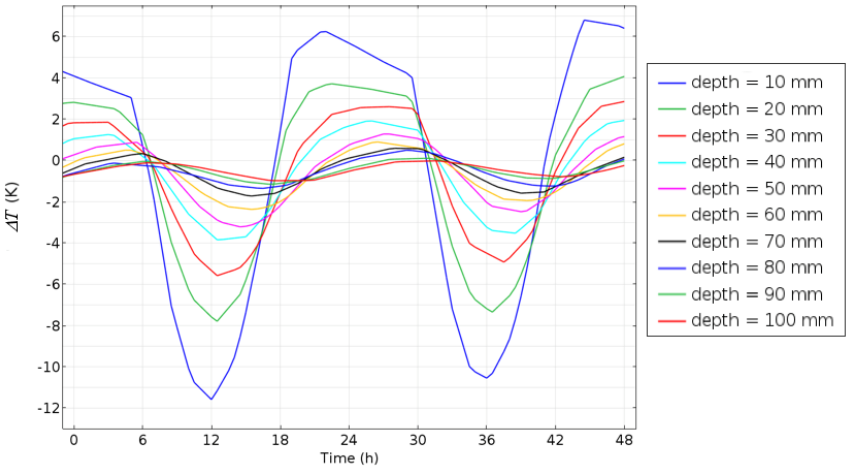

Aluminum sample buried at 10 different depths from the sand surface, extracted from FE simulations. Notice the offset in time of the day of ΔT maxima and minima, as the buried object is placed deeper.

Figure 18. Comparison of the temperature difference between soil above sample and surrounding soil

Figure 19 shows raw images from the camera and its correspondent finite element simulation for a Teflon object emplaced three centimeters deep. We found that FE simulations slightly underestimate the differences in temperature. This can be attributed to the complexity of the heat transfer dynamics between soil, buried object, wooden box, soil where the box is sitting and the surroundings, all included in the model, in combination with the uncertainties of the measured values of the thermal properties of sand and Teflon.

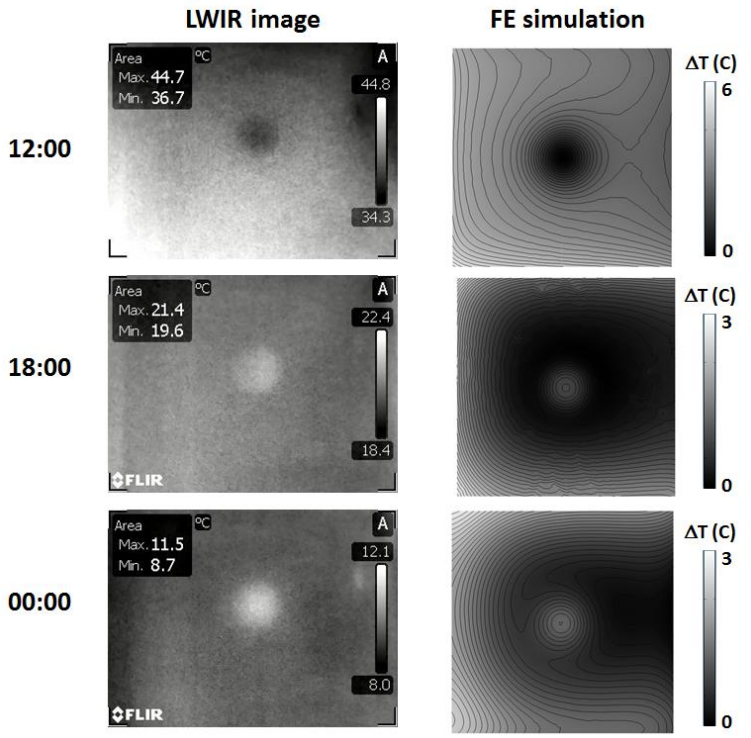

Surface images obtained by an LWIR camera (left) and FE simulations (right) of soil above and soil surrounding a Teflon object buried at 3cm from the sand surface, recorded at 12:00, 18:00 and 0:00 hours.

Figure 19. Comparison between LWIR surface images and FE simulations

The size of the images was selected after testing several fields of view in the camera. It is clear that if the field of view is too large, the ability to resolve the contrast difference is compromised by the other elements in the surroundings. Obviously reducing the field of view limits the area under investigation. In practice, this imaging scheme should use a scanning technique to be able to cover a large area with a small field of view. During the periods where the temperature difference is not significant, such as close to dawn and dusk, some image processing techniques can be applied to improve detection probabilities.

Figures 20 and 21 show images, temperature profile of the center line and transformed intensity (Eq. 2) for data collected at different times of the day for two different burial depths.

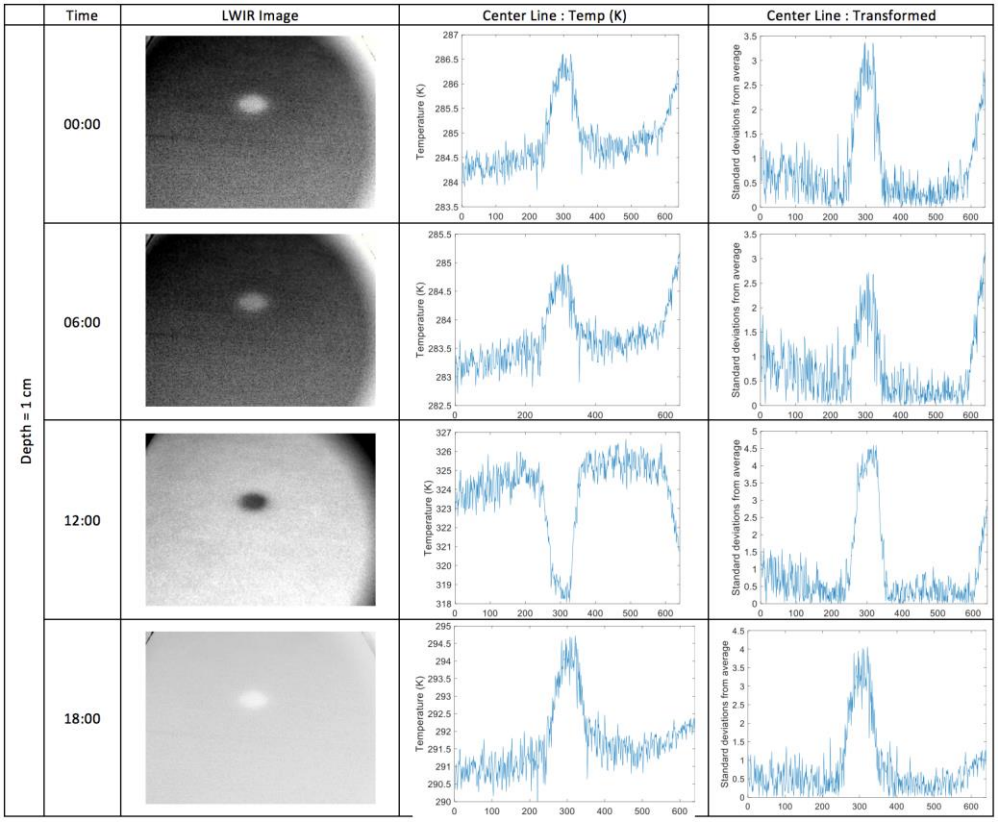

LWIR images (left column), the center line temperature profile (middle column) and transformed intensity profile for an aluminum object buried 1 cm beneath surface.

Figure 20. Table of LWIR images, center line temperature profile, and transformed intensity profile at 1cm depth

Figure 20 shows data and results for an aluminum object buried 1 cm deep. Notice that at very shallow depths it is very easy to detect the buried object on a uniform background. The graphs also show that at dusk and dawn the ΔT is smaller. This becomes more evident for objects buried at greater depths as shown in Figure 21. There, the aluminum object is 8 cm deep and very close to the limits of detection for the LWIR camera and the post-processing used. The selected times are shifted when compared with those in Figure 20, following the trend shown in Figure 18. Since the temperature profile is relatively noisy, an extra step was necessary in order to smooth the observed data. Adjacent average on a window of 15x15 pixels was used and the result is shown by the solid red lines. The smoothing is reflected on the transformed intensity; however, identification of the object remains difficult. The noise shown is more than one order of

magnitude higher than the camera's minimum detectable temperature difference, claimed by the maker to be 20 mK. This indicates the temperature variation is a feature of the soil. Further studies are needed to fully characterize this effect.

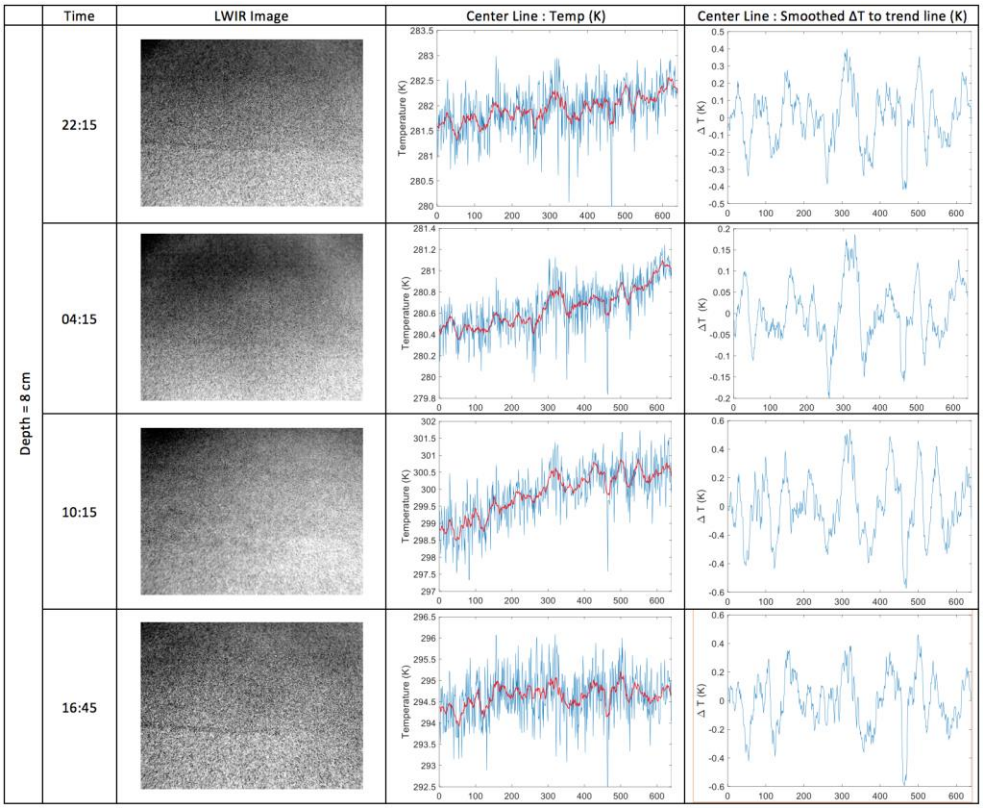

LWIR images (left column), the center line temperature profile (middle column) and transformed intensity profile for a buried aluminum object 8 cm deep.

Figure 21. Table containing LWIR images, center line temperature profile, and transformed intensity profile at 8cm depth

Finally, identification was attempted by programming the algorithm described in the previous section directly into the COMSOL model. Then, parametric sweeps were performed in some of the buried object parameters. Ambient temperature, solar radiation and estimated size of the sample were obtained from the experiment and infrared image. Sand emissivity, density and thermal capacity were kept fixed and the values were obtained from open access databases, according to the region where the soil was extracted. Also, due to the complexity of the problem, specific heat capacity of the buried

simulated object was kept constant at a value that corresponds to an average for man-made material (~ 1000 J/kg.K). The strong constraint here is the burial depth of object. It drastically influences the estimated size and the surface temperature differences used in the detection algorithms. For the proof-of-concept, the depth was kept constant; however, this degree of freedom will be introduced in the next models.

Figure 22 shows the simulated experiment where the infrared image size corresponds exactly to the actual recorded image. The inset shows the temperature profile of the surface line highlighted on the image. Figure 23 shows a comparison between actual and simulated data extracted from the surface center line (figure inset) of the LWIR images taken at 12:00 (noon) when our sample object, a 2 inch diameter aluminum cylinder was buried at one inch deep. Notice that the object is small since the overall environment is scaled down due to the sand box dimensions. This helps to reduce the effects of the box walls on the soil atop the object and its surroundings.

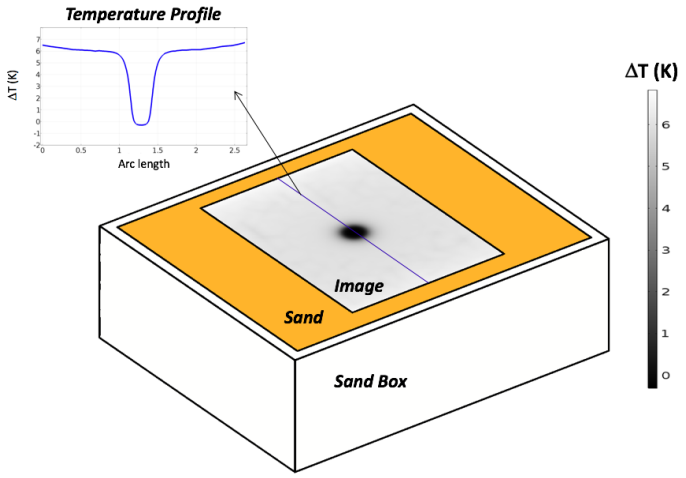

FEM showing the region of interest on the sand box, exactly where the actual infrared images were collected. In the image, dark corresponds to cold and bright to hot. The color bar indicates the temperature difference in the scene. The inset shows the surface temperature profile at the highlighted blue line.

Figure 22. Finite element model surface temperature map

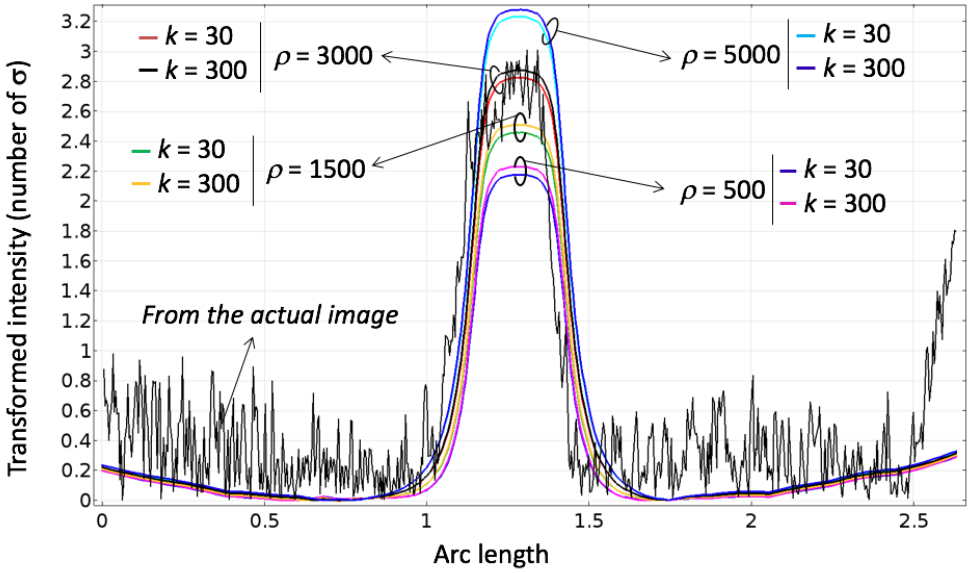

Actual (black line) and simulated (colored lines) surface intensity profile, transformed by the algorithm detailed in the text. The simulated data is provided for different material densities and thermal conductivities. The best match, red and black simulated curves, indicate that the object composition could be a soft metal such as aluminum.

Figure 23. Surface intensity profile transformed by Find Feature algorithm

It is easy to notice in Figure 23 that the density is the dominant parameter in the fitting process. Thermal conductivity has a minor effect for the analyzed conditions. The best fit, red and black curves correspond to densities and thermal conductivities of soft metals and gives an indication that an aluminum object could be the target (k ~ 240 W/ m·K and ρ ~ 2700 kg/m^3). One interesting possibility for this technique is to use the thermal inertia or thermal effusivity ($(k.\rho.C_p)^{1/2}$) to estimate the composition of the buried object [12]. This will be explored in future work.

THIS PAGE INTENTIONALLY LEFT BLANK

V. CONCLUSION

This project explored the ability of detecting near-surface buried objects using infrared surface images. Initial tests performed with long-wavelength infrared camera to obtain surface temperature variation, combined with a finite element modeling show a great potential for actual detection of shallow objects.

A. SUMMARY

Our objective was to determine the impact of IED shape, size, material, burial depth, and time of day on the probability of detection/identification. To better determine the limitations of our thermal IR camera, image acquisition was also carried out with a simulated IED and surrounding soil having similar thermal conductivities.

COMSOL Multiphysics software was used to model heat transport dynamics between the soil, simulated IED, and its surrounding environment. Solar radiation was incorporated in the model based on summer conditions experienced in Monterey, CA in 2017. Finite element modeling provided a reasonable way to obtain insights on what to expect for the actual measurements. LWIR images of the sandbox surface were recorded under environmentally ideal conditions and were used to validate simulation models.

Diurnal behavior was observed in both simulated and experimental datasets and agree with passive IR experimentation discussed in literature. It was found in COMSOL simulation that when the buried object's thermal conductivity is beyond 30 W/(m·K), the daytime temperature difference remains the same. This implies that materials with thermal conductivity in this region, such as aluminum, brass, steel, iron, copper, etc., cannot be identified using this approach.

Post processing techniques applied include elementary transformations operations to enhance collected IR imagery. This, in effect, imposes a standardization routine to all collected IR imagery and enables proper comparisons among image datasets. Lastly, a detection metric for analyzing IR imagery collected was employed to enhance the detection probability.

The developed metric, loosely based on statistical methods, is a multivariate technique (Mahalanobis distance) to detect outliers within a given dataset. While significantly dependent on an array of assumptions, application of this technique with considerably more testing applied, may help generate valuable data to further substantiate classification of a buried objects thermal profile.

B. FUTURE RECOMMENDATIONS

During the course of this study only raw images were used to extract a surface temperature map of the soil under analysis. Modern techniques of image processing have a great potential to improve the detection probability and increase the contrast between the soil layer above the buried object and its surroundings. Also, the introduction of hyperspectral imaging capability that includes SWIR and MWIR bands may add important capabilities toward localization and identification. For the next steps, we suggest studying the fundamentals of combining imaging information of all three infrared bands in order to enhance the detection probabilities of the buried devices. Computational tools are needed to process and enhance images for thermal anomaly detection and subsequent analysis as well as to draw conclusions about the detection of disturbed soil through the moisture and/or air content and granularity. In addition, FE models can be improved to help tune aspects involving spectral fusion and optimize the experimental setup.

The study, also, should be performed using different controlled soils and buried objects. Incorporating surface obstructions and other buried natural elements within the scene would lend to a more realistic model in line with scenes likely presented in an operational environment. Images on all bands should be taken over long periods of time to understand the signature cycle along the day/night period. In addition, heat and mass transfer models could be used to help image interpretation and classification of buried objects signatures.

APPENDIX

The MATLAB m-file that implements the algorithm presented in Figure 3 is given below.

Find_feature.m

```
A = imread('Raw\LWIR-00255.png');  % image file path
B = imadjust(A);   % contrast enhancement
C = mat2gray(B);  % converts pixel values [min max] to [0 1]
c = mean2(C);

if c >= 0.65 % detects if bright background
   C = imcomplement(C);% converts the image to dark background (negative)
   C = imadjust(C); %re-adjusts boundaries through a contrast enhancement
   T = 0.4;% sets threshold to 0.4
else
   T = 0.6; % dark background, sets threshold to 0.6
end

bkgrd = imopen(C,strel('disk',50,8)); % finds the background using a morphological
opening - structuring element disk of 50 pixel diam.
D = mat2gray(double(C)-double(bkgrd)); % remove background; attempt to equalize
illumination non-uniformities using the morphological reconstruction
w25 = fspecial('average',[25 25]); % creates a smoothing (average) filtering mask for the
image (granularity reduction)
E = imfilter(D,w25,'symmetric');  % implements the convolutional filtering of the image
using the mask above.
F = imbinarize(E,T);  % image thresholding
G = bwareaopen(F,30); % removes 'salt noise' perhaps due to thresholding and
granularity

figure
imshow(B) % shows original image (contrast enhanced, but preserving original
background polarity)
hold on   % prepares image for detected feature contour overlay
H = bwboundaries(G); % finds the boundaries between detected feature (logical 1) and
background (logical 0)
for k = 1:length(H) % feature contour overlay routine
   boundary = H{k};
   plot(boundary(:,2), boundary(:,1), 'g', 'LineWidth', 2)  % contour plot
end % end routine
 hold off % turns overlay off
```

THIS PAGE INTENTIONALLY LEFT BLANK

LIST OF REFERENCES

[1] T. Hanshaw, "Multi-sensor fusion for detection of mines and 'mine-like' targets," in *Proc. SPIE 2496, Detection Technologies for Mines and Minelike Targets*, 1995. [Online]. doi: 10.1117/12.211311

[2] A. W. Fountain, J. A. Guicheteau, W. F. Pearman, T. H. Chyba, and S. D. Christesen, "Long-range standoff detection of chemical, biological, and explosive hazards on surfaces," in *Proc. of SPIE 7679, Micro- and Nanotechnology Sensors, Systems, and Applications II*, Orlando, 2010. [Online]. doi: 10.1117/12.851785

[3] National Research Council Staff, *Existing and Potential Standoff Explosives Detection Techniques*, Washington, DC: National Academies Press, 2004. [Online] Available:http://ebookcentral.proquest.com/lib/ebook-nps/detail.action?docID=3376734.

[4] A. A. Faust, C. J. de Ruiter, A. Ehlerding, J. E. McFee and E. Svinsas, "Observations on military exploitation of explosives detection technologies," in *Proc. of SPIE 8017, Detection and Sensing of Mines, Explosive Objects, and Obscured Targets XVI*, 2011. [Online]. doi: 10.1117/12.886391

[5] J. Apostolos, W. Mouyos, J. Feng, and W. Chase, "Low-power stimulated emission nuclear quadrupole resonance detection system utilizing Rabi transistions," in *Proc. of SPIE 8709, Detection and Sensing of Mines, Explosive Objects and Obscured Targets XVIII*, Baltimore, 2013. [Online]. doi: 10.1117/12.2021508

[6] C. Hibbitts , J. Staszewski , A. Cempa, V. Sha and S. Abraham, "Optical cues for buried mine detection," in *Proc. of SPIE 7303, Detection and Sensing of Mines, Explosive Objects, and Obscured Targets XIV*, Orlando, 2009. [Online]. doi: 10.1117/12.818753

[7] F. Shubitidze, J. P. Fernandez, I. Shamatava, B. E. Barrowes and K. O'Neill, "Target-classification approach applied to active UXO," in *Proc. of SPIE 8709, Detection and Sensing of Mines, Explosive Objects, and Obscured Targets XVIII*, Baltimore, 2013. [Online]. doi: 10.1117/12.2016351

[8] N. C. Rowe, S. Gurminder, J. Sundram, P.P. Sim, "Assessment of Electromagnetic and Passive Diffuse Infrared Sensors in Detection of IED-Related Behavior / 13th ICCRTS: C2 for Complex Endeavors," Conference Paper, Dept. of Computer Science, NPS, Monterey, CA, USA, 2008. [Online]. Available: http://hdl.handle.net/10945/35994

[9] K. H. Ghazali and M. S. Jadin, "Detection Improvised Explosive Device (IED) Emplacement Using Infrared Image," in *IEEE Computer Modelling and Simulation,* 2014. doi: 10.1109/UKSim.2014.111

[10] K. Khanafer and K. Vafai, "Thermal Analysis of Buried Land Mines Over a Diurnal Cycle," *IEEE Transactions on Geoscience and Remote Sensing*, vol. 40, no. 2, pp. 461–473, Feb. 2002. [Online]. doi: 10.1109/36.992811

[11] J. Simunek, M. H. Hendrickx, and B. Borchers, "Modeling transient temperature distributions around landmines in homogeneous bare soils," in *Proc of SPIE 4394, Detection and Remediation Technology Mines Minelike Targets VI*, Orlando, 2001. [Online]. doi: 10.1117/12.445490

[12] S. Howington, M. Ginsberg and G. Koh, "Water flow and distribution around buried landmines," in *Proc. of SPIE 6217, Detection and Remediation Technologies for Mines and Minelike Targets XI,* Orlando, 2006. [Online]. doi: 10.1117/12.666375

[13] K. Stone, J. M. Keller, M. Popescu and C. J. Spain, "Buried explosive hazard detection using forward-looking long-wave infrared imagery," in *Proc of SPIE 8017, Detection and Sensing of Mines, Explosive Objects, and Obscured Targets XVI,* Orlando, 2011. [Online]. doi: 10.1117/12.886673

[14] A. P. Bowman, E. M. Winter, A. D. Stocker and P. G. Lucey, "Hyperspectral infrared techniques for buried landmine detection," in IEEE *Detection of Abandoned Land Mines*, Edinburg, UK, 1998. doi: 10.1049/cp:19980704

[15] A. T. DePersia, A. P. Bowman, E. M. Winter and P. G. Lucey, "Phenomenology considerations for hyperspectral mine detection," *in Proc. of SPIE 2496, Detection Technologies for Mines and Minelike Targets,* Orlando, 1995. [Online]. doi: 10.1117/12.211312

[16] R. L. van Dam, B. Borchers, J. M. H. Hendrickx and S. Hong, "Soil effects on thermal signatures of buried nometallic landmines," in *Proc of SPIE 5089, Detection and Remediation Technologies for Mines and Minelike Targets VIII,* Orlando, 2003. [Online]. doi: 10.1117/12.487205

[17] J.-R. Simard, "Improved Landmine Detection Capability (IDLC): Systematic approach to the detection of buried mines using passive IR imaging," in *Proc of SPIE 2765, Detection and Remediation Technologies for Mines and Minelike Targets,* Orlando, 1996. [Online]. doi: 10.1117/12.241251

[18] S. Hong, T. W. Miller, B. Borchers, J. M. Hendrickx, H. A. Lensen and S. P. Van Den Broek, "Land mine detection in bare soils using thermal infrared sensors," in *Proc. of SPIE 4742, Detection and Remediation Technologies for Mines and Minelike Targets VII,* Orlando, 2002. [Online]. doi: 10.1117/12.479124

[19] F. Cremer, J. Schavemaker, W. de Jong and K. Schutte, “Comparison of vehicle-mounted forward-looking polarimetric infrared and downward-looking infrared sensors for landmine detection,” in *Proc. of SPIE 5089, Detection and Remediation Technologies for Mines and Minelike Targets VIII*, 2003. [Online]. doi: 10.1117/12.487823

[20] R. Garcia-Padron, D. Loyd and S. Sjokvist, “Heat and moisture transfer in wet sand exposed to solar radiation--models and experiments concerning buried objects,” *Subsurface Sensors Technology Applications*, vol. 3, no. 2, pp. 125–150, April 2002.

THIS PAGE INTENTIONALLY LEFT BLANK

INITIAL DISTRIBUTION LIST

1. Defense Technical Information Center
   Ft. Belvoir, Virginia

2. Dudley Knox Library
   Naval Postgraduate School
   Monterey, California